ISSN 0031-918X, Physics of Metals and Metallography, 2018, Vol. 119, No. 1, pp. 60–68. © Pleiades Publishing, Ltd., 2018.
Published in Russian in Fizika Metallov i Metallovedenie, 2018, Vol. 119, No. 1, pp. 63–72.

STRENGTH AND PLASTICITY

Comparing Microstructures and Tensile Properties of Intercritically Annealed and Quenched-Tempered 1.7Ni–1.5Cu–0.5Mo–0.2C Powder Metallurgy Steels[1]

Ahmet Güral[a], *, Hüdayim Başak[b], and Mustafa Türkan[c]

[a] *Department of Metallurgical and Materials Engineering, Technology Faculty, Gazi University, Ankara, Turkey*
[b] *Department of Industrial Design Engineering, Technology Faculty, Gazi University, Ankara, Turkey*
[c] *Graduate School of Natural and Applied Sciences, Gazi University, Ankara, Turkey*
**e-mail: agural@gazi.edu.tr*

Received October 11, 2016; in final form, November 17, 2016

Abstract—The aim of this study was to compare the influence of intercritical quenching (IQ), step quenching (SQ) and quenching plus tempering (QT) heat treatments on the microstructure and tensile properties of 1.7Ni–1.5Cu–0.5Mo–0.2C pre-alloyed powder metallurgy (P/M) steels. In the microstructures of the IQ and SQ specimens partial martensite having Ni-rich phases formed up in the soft ferritic matrix. It was observed that unlike Mo, a Cu alloying element dissolved homogeneously in the specimens. The martensite volume fraction (MVF) in the SQ specimens was higher than that in the IQ specimens. It was found that macrohardness, yield and tensile strengths increased, whereas microhardness of ferrite and elongation decreased with increasing MVF. However, with this increase, microhardness values of martensite phases decreased in the IQ specimen, while they increased in SQ specimens. It was observed that the yield, tensile, and elongation values of the QT specimens were lower than those of all intercritically annealed specimens having the same hardness values.

Keywords: powder metallurgy, tensile properties, intercritical annealing, dual phase microstructure, ferrite plus martensite

DOI: 10.1134/S0031918X18010027

INTRODUCTION

Alloying elements have been widely used to improve the mechanical properties of powder metallurgy (P/M) parts [1–3]. However, alloying elements added by conventional P/M production routes may not disperse and solve homogeneously in the matrix structure during sintering process. A microstructure of P/M steels could exhibit a heterogeneous distribution due to the density, particle morphology, and dimension variety of alloying powders admixed to the main powder. The use of diffusion bonded or master alloyed powders are much more suitable for homogenizing of a microstructure in P/M steels.

It is well known that many mechanical properties of P/M steels can be improved by various heat treatments [5–7]. The quenching and tempering process is commonly applied to improve mechanical properties of P/M steels [3]. Therefore, coexistence of soft and hard phases in the microstructure is significant for optimization of tensile strength and ductility [1–4]. In earlier studies, intercritical annealing (ICA) and austempering heat treatments [8, 9] were applied to P/M steels, as well as quenching plus tempering heat treatments. In addition, the tensile [10, 11], impact toughness [12, 13], and wear [14] properties of the plain carbon P/M steels that had undergone different heat treatments were also investigated.

Dual-phase microstructures containing mainly the ferrite plus martensite constituent produced by ICA heat treatments are materials that have better ultimate strength, ductility, toughness, and higher strain hardening and deformability than conventional low carbon steels [15, 16]. Low-alloy hypoeutectoid steels are intercritically annealed between the Ac_1 and Ac_3 temperatures to produce a mixture of ferrite and austenite. After that, a ferrite plus martensite dual-phase structure is produced by quenching from ICA region. The mechanical performance of dual-phase steels containing ferrite plus martensite can be optimized by controlling the shape, size, amount, and distribution of the martensite in the ferritic matrix [2, 17–21].

In the present study, microstructural and tensile properties of 1.7N–1.5Cu–0.5Mo diffusion bonded pre-alloyed iron based P/M steels that had passed

[1] The article is published in the original.

through conventional quenching-tempering and ICA heat treatment processes were examined and compared.

EXPERIMENTAL

The specimens were prepared by adding the graphite (UF4) by weight of 0.2% used as the carbon source and the amide wax by weight of 0.91% as the lubricant to diffusion bonded alloy powder of composition 1.5Cu–1.74Ni–0.5Mo (ferrous based Höganäs Distaloy AB). After the powders were homogeneously mixed, the mixed powders was shaped under 670 MPa pressing pressure at room temperature in a mould in accordance with the requirements of ASTM-E 8M tensile test standard [22]. The specimens removed from the mould were sintered at 1250°C under an atmosphere of high purity argon gas for 30 minutes.

The IQ heat treatment of the first group of sintered specimens was carried out by directly applying an intercritical annealing at different temperatures (705–735–765°C) with the subsequent rapid oil-quenching. The specimens subjected to this heat treatment cycle were marked as IQ705, IQ735 and IQ765, respectively according to the ICA temperatures (Fig. 1a).

The SQ heat treatment was applied to another group of sintered specimens. After austenization at 890°C, these specimens were cooled down at three different inctercritical annealing temperatures (705–735–765°C) and oil quenched subsequently (Fig. 1b). The specimens produced in this way were mark-labelled as SQ705, SQ735, and SQ765, respectively according to the applied temperatures. The ferrite plus martensite microstructure combination was aimed for the specimens of both IQ and SQ series.

Finally, in order to compare the tensile properties, the quenching + tempering (QT) heat treatments were applied to the third group of specimens. These specimens were austenitized at 890°C for 10 minutes and then rapidly oil quenched. Some of these specimens were tempered at 180°C for 2 hours and the others were tempered at 250°C for 3 hours (Fig. 1c). The specimens were labelled as QT180 and QT250, respectively.

The specimens were etched with the 2% nital solution after the grinding and polishing processes for the microstructural analyses. JEOL JSM-6060LV scanning electron microscopy (SEM) was used for these analyses. To determine the dispersion of the Ni, Cu, and Mo elements in the microstructure, elemental mapping analysis was performed using SEM with an energy dispersive X-ray spectrometry (EDS) attachment. After IQ and SQ heat treatments, the linear intercept method was used to calculate the MVF in the microstructure. Hardness Rockwell C (HRC) values were measured by using an Instron-Wolpert 7551 hardness tester. Microhardness values of the ferrite and martensite phases in the dual phase microstructure were determined with the help of a Vickers tester (Shimadzu HMV-2) using 10 g load. Tensile tests were carried out at a crosshead speed of 5 mm min^{-1} using a universal Shimadzu testing machine with 5 kN tensile test capacity, at room temperature.

RESULTS AND DISCUSSION

SEM microstructure images of the sintered P/M specimens are given in Fig. 2. In Fig. 2a, the pearlitic structures (white regions), the ferrite matrix, and the internal pores in the low magnification microstructure are seen. As can be obviously seen in a high-magnification microstructure in Fig. 2b, the pearlitic structures had a divorced morphology. This formation is a general characteristic of Ni-containing ferrous sintered P/M steels [23]. It can be speculated that a considerable amount of C from added graphite dissolved in Ni-rich austenitic zones of concentration while the remaining C formed the divorced pearlitic zones.

After IQ and SQ heat treatments, Ni-rich martensite islands in the ferritic matrix were obtained as seen in Figure 3 and 4, respectively. It was surprising that even at 705°C, partial Ni-rich martensite phases in the ferritic matrix occurred in the IQ and SQ specimens. The Ac_1 temperature in the P/M specimens was 692°C in the preliminary studies. Whereas, Ac_1 and Ac_3 temperatures in these specimens were determined as 711 and 808°C, respectively according to Andrew's empirical formula [24].

Due to their high Ni content, Ni-rich regions were primarily austenitized in at ICA temperature. Therefore, the zones with lower Ni around the Ni-rich regions were partially austenitized into ferrite until they reach equilibrium at the constant ICA temperature. After the quenching process, while Ni-Rich regions remained austenitic at room temperature, austenite phases with lower Ni concentration around the Ni-rich austenitic areas transformed into martensitic phases in the ferritic matrix.

The microstructure images of the QT180 and QT250 specimens are shown in Figs. 5a, 5b, respectively. Typically tempered martensitic matrix structures occurred in both specimens. Ni-rich regions occurred in the martensitic matrix in the QT specimens (Fig. 5). It was observed that the amount of the martensite plates decreased in the microstructure of QT250 specimens. The martensitic transformation didn't occurred because these zones remained austenitic after quenching due to the high concentration of Ni.

Figure 6 provides the relationship between ICA temperature and MVF in dual phase P/M specimens containing ferrite plus martensite microstructures produced through both methods. MVF also increased with the increase in ICA temperature in the specimens. While the MVF was ~30% in the IQ705 and SQ705 specimens, in the IQ765 and SQ765 specimens quenched at 765°C, it was 62 and 67%, respectively.

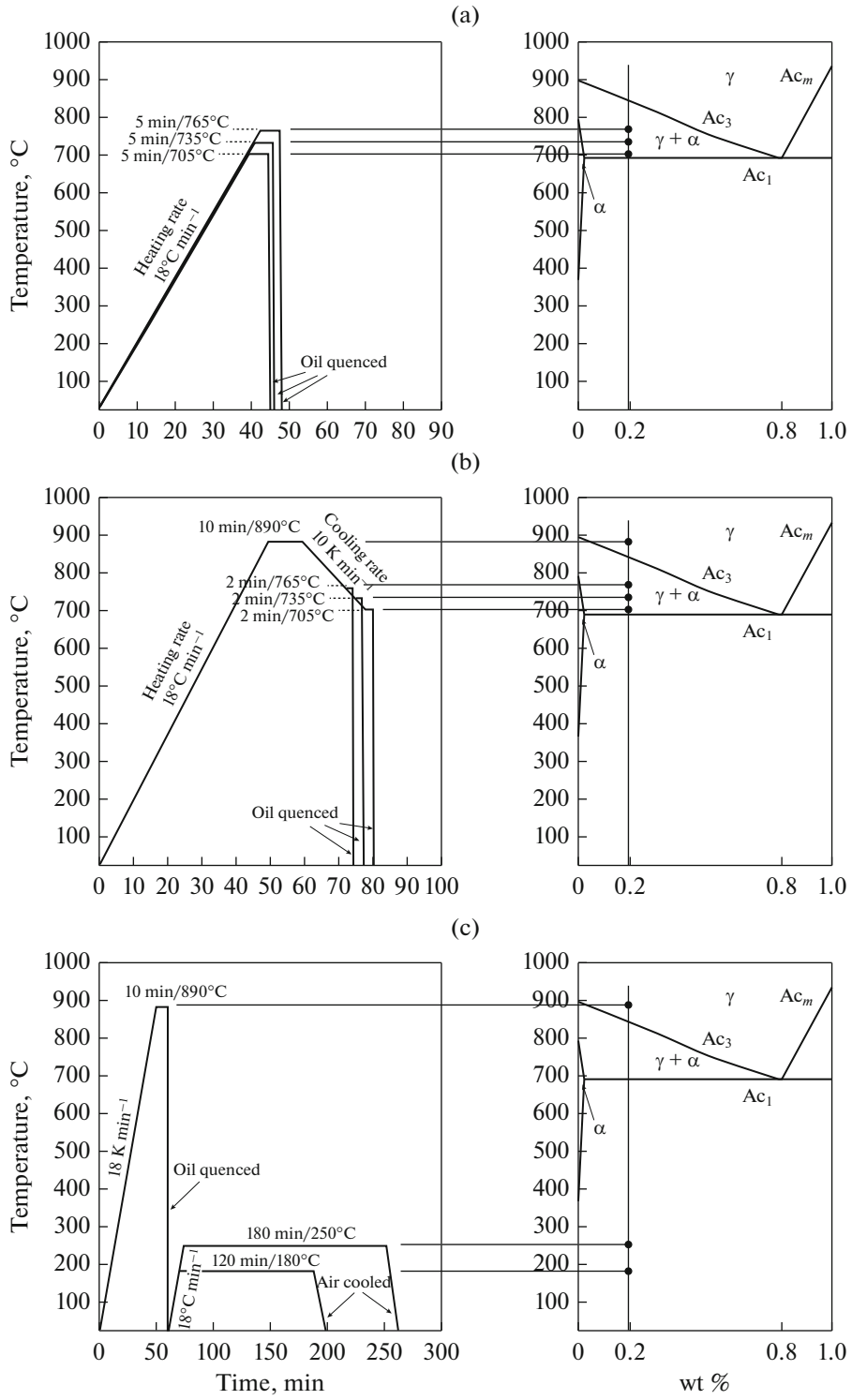

Fig. 1. Schematic illustrations of applied different heat treatment cycles; (a) intercritical quenching (IQ), (b) step quenching (SQ), (c) quenching and tempering (QT).

The holding period of the SQ specimens at the ICA region was shorter than that of the IQ specimens. Thus, a higher MVF fraction was obtained in the SQ specimens in comparison to the IQ specimens when quenched.

EDS element mapping analysis of the dispersion of alloying elements in the IQ765, SQ765, and QT180 specimens are given in Figs. 7a–7c, respectively. It can be seen in Figs. 7a, 7b that although undissolved Mo existed in the pores among sintered particles in all

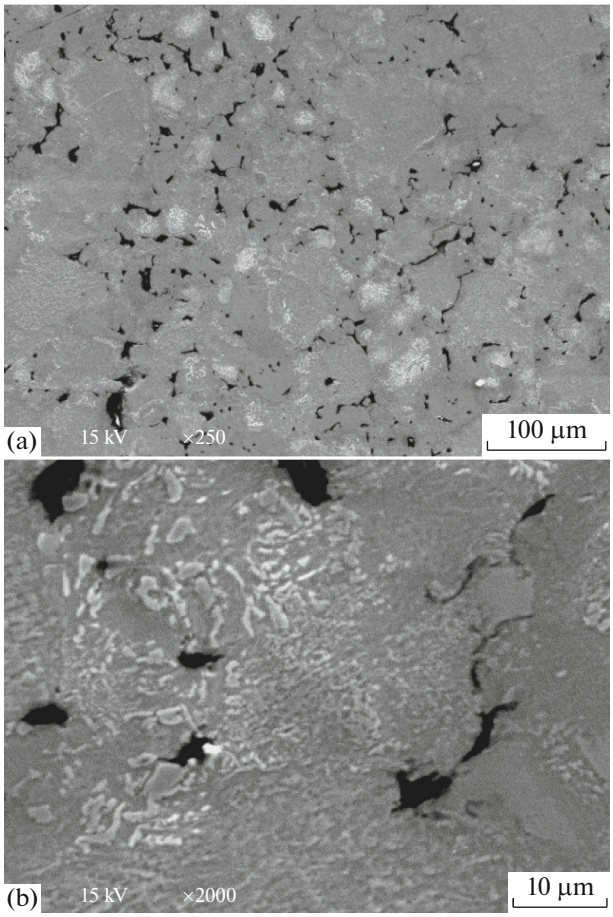

Fig. 2. Microstructures of sintered specimens: magnifications are (a) 250× and (b) 2000×.

specimens, Cu and Ni dispersed particularly within the martensite phases. In the SQ765 and IQ765 specimens, it was also observed that Cu was dispersed more homogeneously in the microstructure than Ni.

It can be seen in the Fig. 7c that in the QT180 specimen, Ni-rich regions were dispersed in martensitic microstructures. Ni-rich regions didn't transform into martensitic structures and remained austenitic in the martensitic matrix.

The sintered density was 7.2 g cm^{-3} and the relative densification fraction was 0.92. When the densification values of the specimens to which heat treatemnts were applied increased more than the densities of the specimens that were only sintered (Table 1), it can be speculated that the expansion in the volume of the martensite during transformation from austenite to martensite led the pores to shrink, which in turn caused the density to increase. This effect was stronger in QT specimens. In this study, it was seen that pores occurred in two different zones. The first one, as is seen in Fig. 3a, it is when the chemical bonds were formed among filings during the sintering process and the pores are isolated.

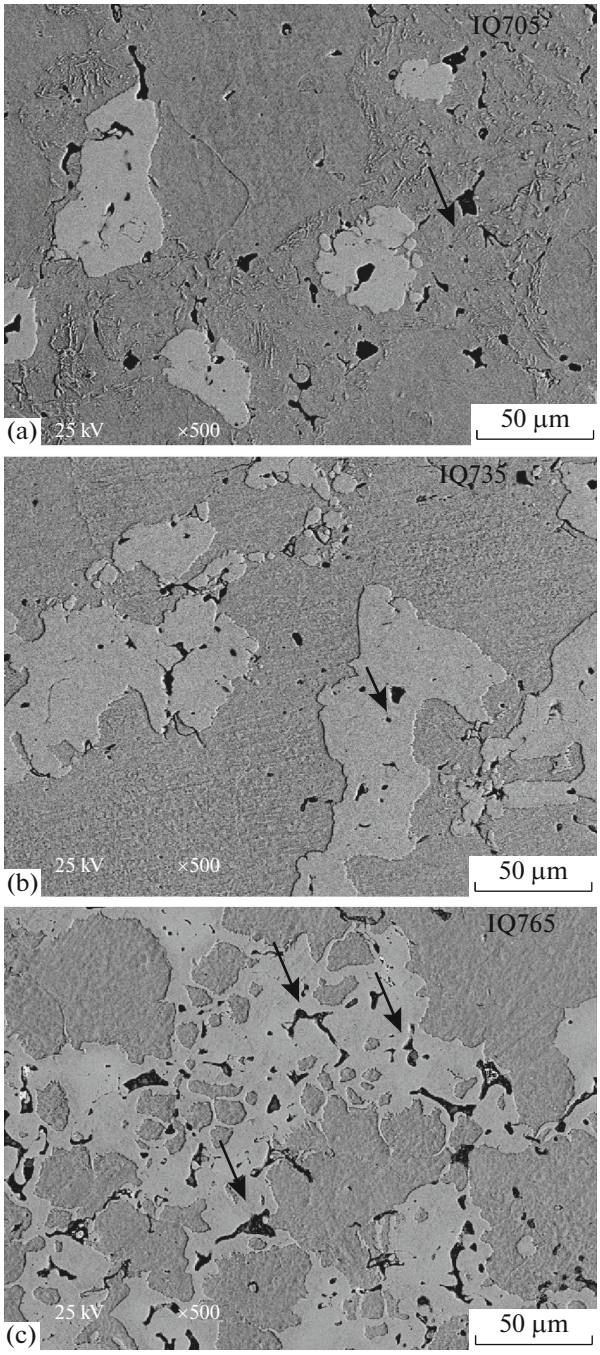

Fig. 3. Microstructures of IQ series specimens formed at different intercritical annealing temperatures. (In the images: light grey, grey, and black areas are martensite, ferrite, and pores, respectively.)

As for the other pore formation, they are pores or cavities that occur in the middle of the martensite phases (light grey zones) indicated by the arrow in the microstructure images in Figs. 3b, 3c. The pores in Fig. 3c are different from the ones in Fig. 3b. The pores (in the middle of the martensite) in the Fig. 3c are thought to have occurred as a result of the diffusion

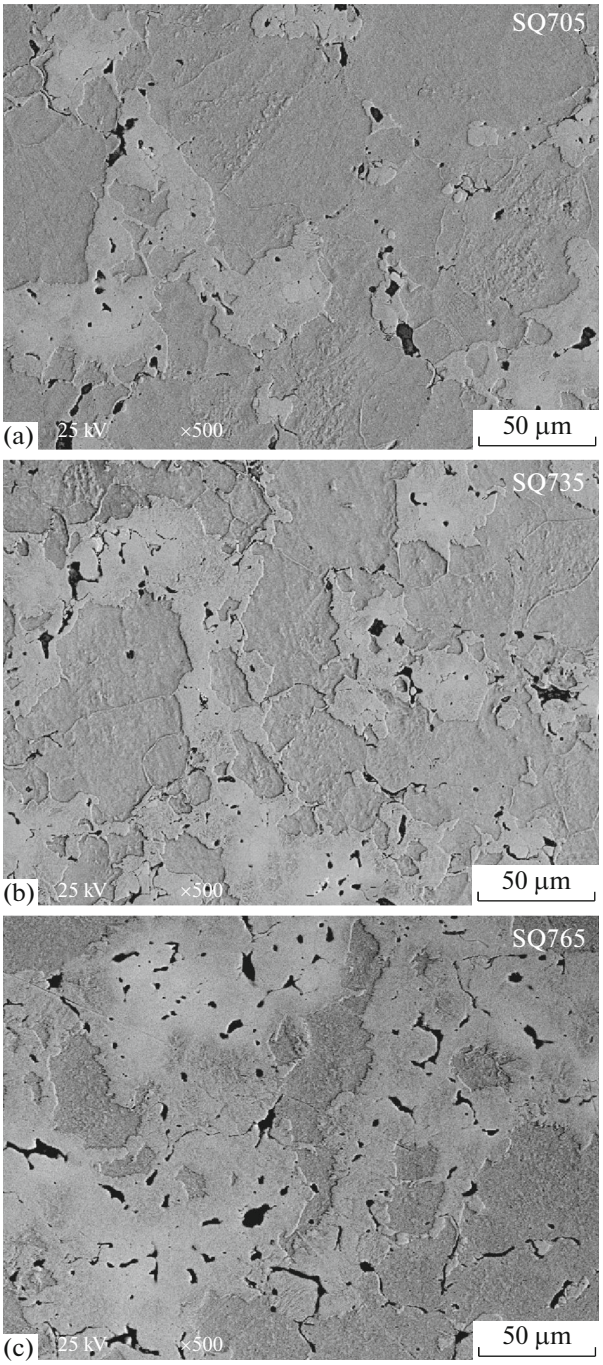

Fig. 4. Microstructures of SQ series specimens formed at different intercritically annealing temperatures, after ful austenization. (In the images: light grey, grey, and black areas are martensite, ferrite, and pores, respectively).

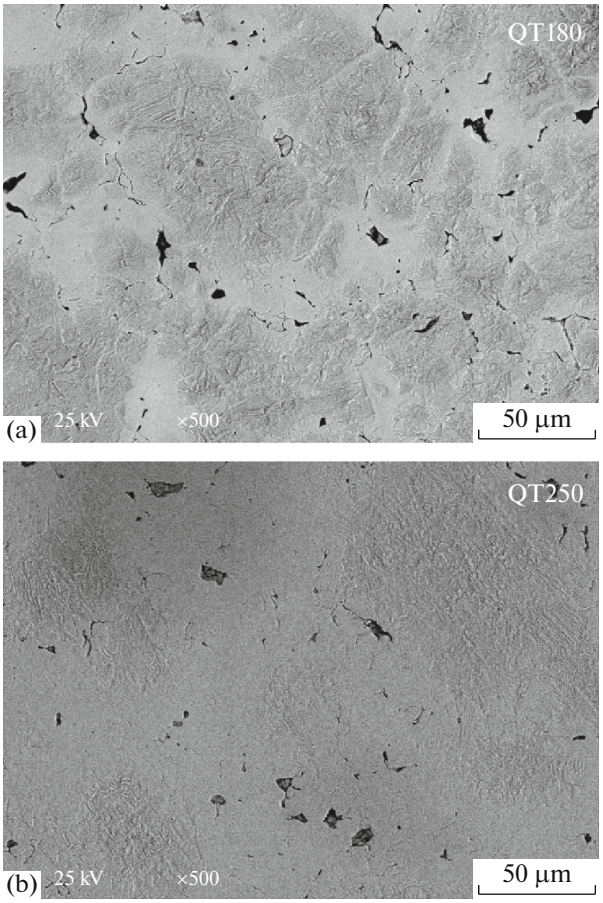

Fig. 5. Microstructures of quenched and tempered specimens (a) QT180 and (b) QT250.

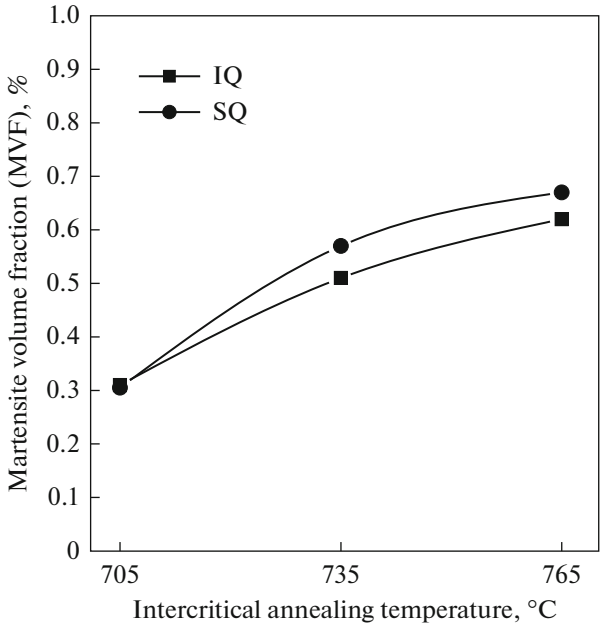

Fig. 6. MVF variation in the IQ and SQ series specimens according to ICA temperatures.

of the nickel element towards the austenite phase formed during the ICA.

Macro- and micro-hardness values of specimens are given in Table 1. The macro-hardness values of the IQ and SQ specimens increased with the increase in ICA temperature. It was observed that the hardness of

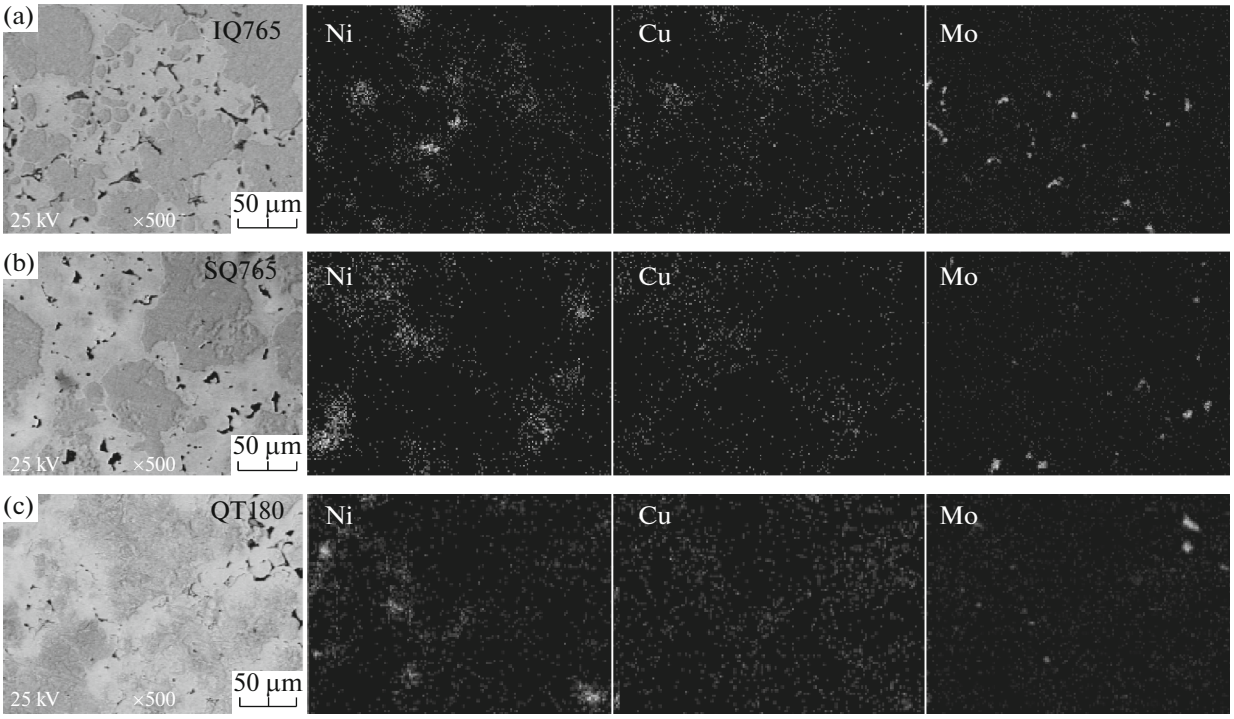

Fig. 7. Distributions of Ni, Cu, and Mo elements in the microstructures of (a) IQ765, (b) SQ765, and (c) QT180 specimens, respectively mapped by EDS analysis.

SQ specimens at a constant ICA temperature was higher than that of the IQ specimens due to the SQ specimens' higher MVF. The micro-hardness of the ferrite phases of the IQ and SQ specimens increased as ICA temperature increased. However, the hardness of the ferrite phase in the SQ specimens were lower than those of the IQ specimens. While the micro-hardness of martensite phases decreased in the IQ specimens, it increased in the SQ specimens as the ICA temperature increased. This can be attributed to the amount of dissolved nickel in the martensite phase increased in the SQ specimens with the increase in ICA temperature.

Tensile values of the specimens are given in Table 1. Yield and tensile values of the sintered specimens were low because their microstructure had a ferrite plus pearlite structure. While the tensile strengths of the specimens to which IQ and SQ heat treatments were applied increased depending on the increasing MFV, their ductility values decreased. An increase in the ICA temperature leads to an increase in MVF as well as to a decrease in the C content of martensite. Due to increasing MVF, the yield and tensile strengths of the intercritically annealed specimens increased, but consequently their ductility decreased. Tensile load

Table 1. The density, hardness and tensile properties of the specimens

Specimens	Density, g cm^{-3}	Hardness, *HRC*	Microhadness, $HV_{0.01}$		Yield strength, MPa	Ultimate tensile strength, MPa	Relative ultimate elongation, %
			ferrite	martensite			
Sintered	7.19	*	–	–	292	383	3.14
IQ705	7.25	24	235	758	322	459	2.82
IQ735	7.26	25	195	600	403	520	2.10
IQ765	7.25	32	185	535	408	541	1.59
SQ705	7.28	24	173	264	405	555	3,56
SQ735	7.26	29	165	310	453	624	3.42
SQ765	7.26	34	155	338	476	710	3,38
QT180	7.31	33	–	–	394	659	2.54
QT250	7.42	22	–	–	336	498	3.31

* Hardness of sintered specimen is 74 HRB.

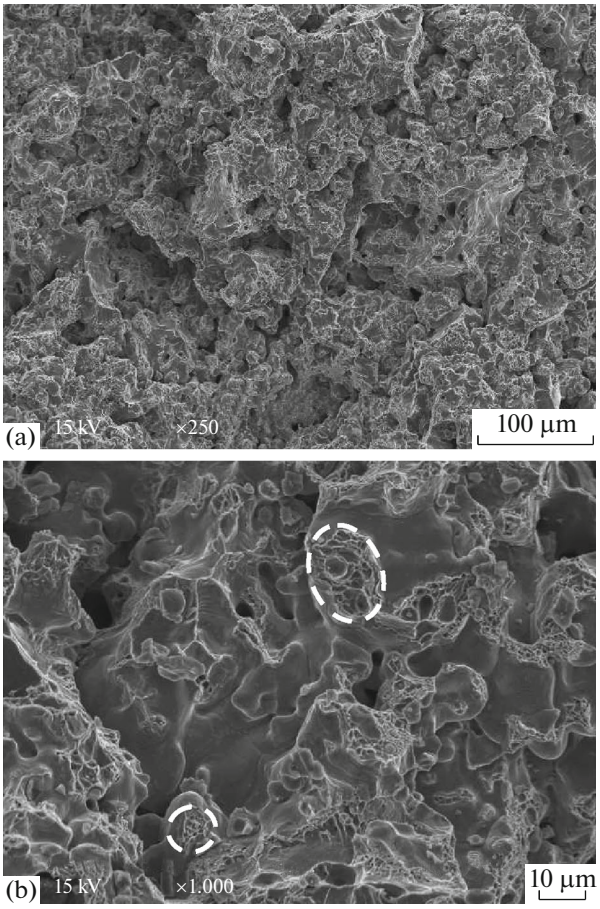

Fig. 8. Fracture surface morphologies of sintered specimens: Magnifications are (a) 250×, (b) 1000×.

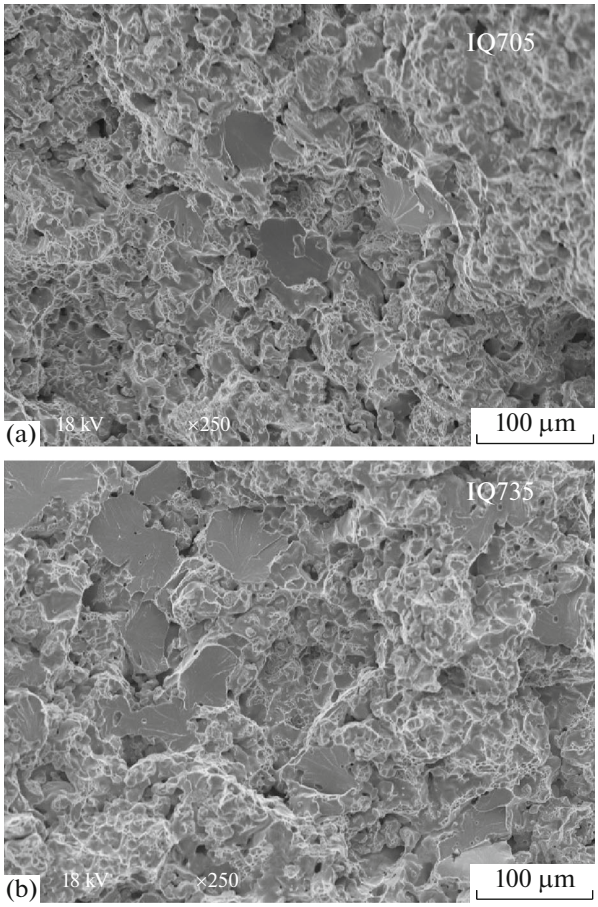

Fig. 9. Fracture surface morphologies of directly intercitical annealed specimens; (a) IQ705, (b) IQ735.

applied to the P/M materials that do not have high density is experienced by the necks of the sintered powder particles. This reduces the effective load bearing capacity. Micro-plastic dimple morphologies seen in the sintering necks (Fig. 8) confirm this case.

SQ specimens were of more yield and tensile strength compared to IQ specimens at the constant ICA temperature. When IQ705, SQ705, and QT250 specimens, which had the lowest hardness value of ~22–24 *HRC,* were analysed, the yield and tensile stress and fracture elongation of the SQ705 specimens were greater than in the case of the IQ705 and QT250 specimens. On the other hand, the SQ765 specimen had the highest yield, tensile stress and fracture elongation values among the specimens which had ~33–34 *HRC* hardness value. According to these results, the yield, tensile stress properties and fracture elongation properties were improved further through the SQ heat treatments in comparison to the QT and IQ heat treatments. The presence of the ferrite phase at the grain boundaries in the SQ specimens can be considered as the most important feature affecting the tensile properties.

After tensile testing analyses, localized dimple fracture modes were observed in the soft ferritic matrix in the sintered specimen (Fig. 8). These ductile fractures have occurred locally in small quantities in the sintering neck bonds (in the dashed circle in the Fig. 8b). The fracture surface images of the IQ, SQ, and QT specimens are given in the Figs. 9–11, respectively. Dimple-type and cleavage-type fractures occurred in the specimens that went through IQ and SQ heat treatments (Figs. 9 and 10). The SQ specimens were observed to have more cleavage-type fracture facets than the other specimens and to show further tendency to increase with high MVF. It can be speculated that this was the result of the martensite islands formation of connectivity with the increase of martensite phase (Figs. 3, 4). The fractures occurred in the form of cleavage because the network that shaped hard martensite phase limited the ductility. While the cleavage fracture zones in the IQ specimens increased with the increase in MFV, these zones tended to decrease in the SQ specimens. In the QT180 and QT250 heat treatment specimens, completely dimple-type fractures occurred in their microstructures instead of cleavage-type fractures (Fig. 11). At the same time, micro dimple-type

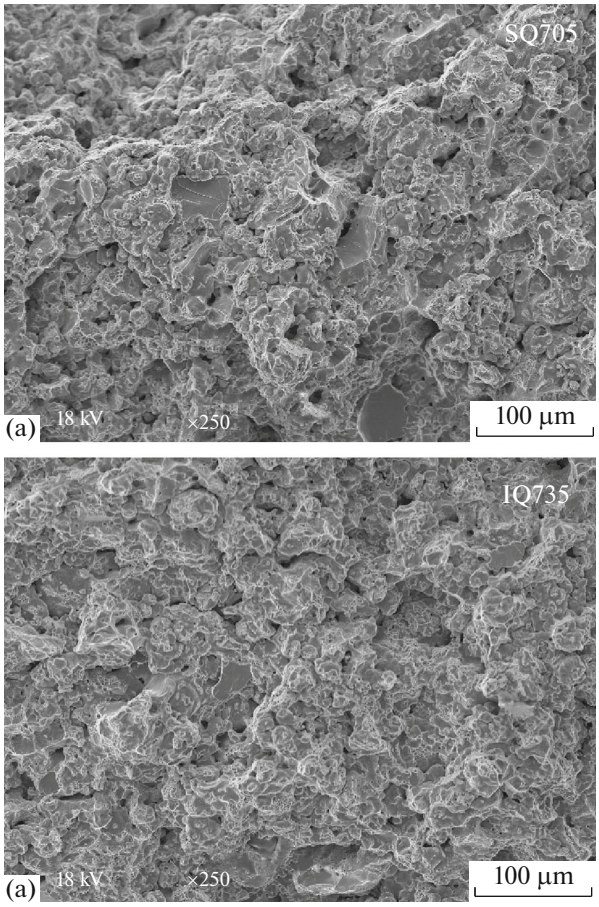

Fig. 10. Fracture surface morphologies of (a) IQ705 and (b) IQ735 specimens.

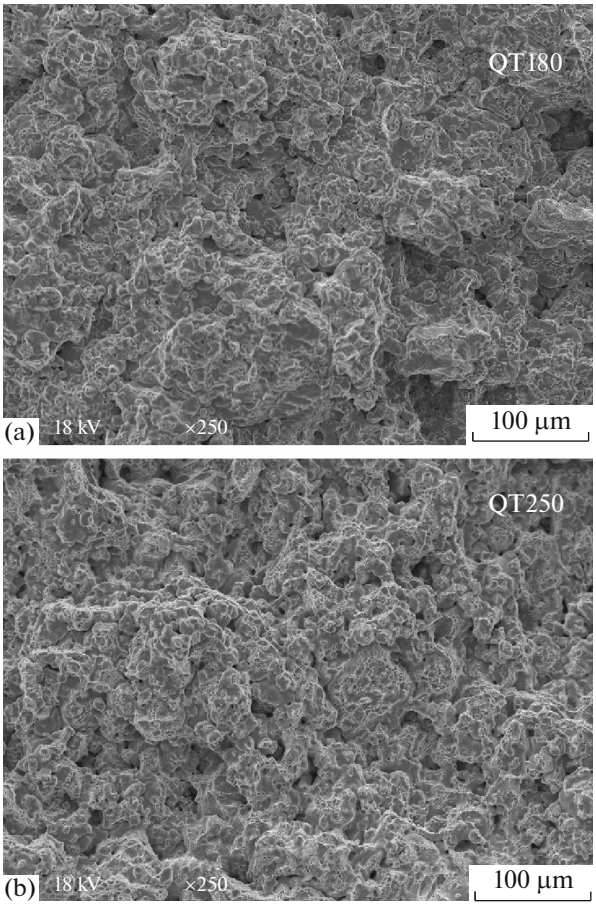

Fig. 11. Fracture surface morphologies of quenched and tempered specimens; (a) QT180, (b) QT250.

fracture modes were observed owing to the fact that the carbon content of the martensite produced in QT specimens was lower than the carbon content of the martensite produced in IQ and SQ specimens.

CONCLUSIONS

The divorced pearlitic microstructure was produced around the Ni-rich areas in the ferritic matrix under sintering conditions. Ni-rich areas in the martensitic matrix was formed in the quenched and tempered specimens. Ni-rich martensite phases in the ferritic matrix were produced through ICA heat treatments.

The macrohardness values of the P/M specimens and the volume fraction of martensite increased with increasing ICA temperature. While the micro-hardness of the martensite phase in the IQ specimens decreased with the increase in ICA temperature, this value showed an increase in the SQ specimens. The microhardness values of the martensite phase were higher in the IQ specimens in comparison with the other specimens. The microhardness of the ferrite phase decreased with ICA temperature in all specimens.

When IQ705, SQ705, and QT250 specimens, which had the lowest hardness value of ~22–24 *HRC* were analysed, the yield and tensile stress and fracture elongation of the SQ705 specimens were higher than in the case of the IQ705 and QT250 specimens. On the other hand, the SQ765 specimen had the highest yield, tensile stress and fracture elongation values among the specimens that had ~33–34 *HRC* hardness value. According to these results, the yield, tensile stress properties and fracture elongation properties were improved further through the SQ heat treatments in comparison with the QT and IQ heat treatments.

REFERENCES

1. K. S. Narasimhan, “Sintering of powder mixtures and the growth of ferrous powder metallurgy,” Mater. Chem. Phys. **67**, 56–65 (2001).
2. M. W. Wu, L. C. Tsao, G. J. Shu, and B. H. Lin, “The effects of alloying elements and microstructure on the impact toughness of powder metal steels,” Mater. Sci. Eng., A **538,** 135–144 (2012).
3. M. W. Wu, G. J. Shu, and S. Y. Chang, “A novel Ni-containing powder metallurgy steel with ultrahigh

impact, fatigue, and tensile properties," Metallurg. Mater. Trans. A **45**, 3866–3875 (2014).

4. B. A. Gething, D. F. Heaney, D. A. Kossa, and T. J. Mueller, "The effect of nickel on the mechanical behaviour of molybdenum P/M steels," Mater. Sci. Eng., A **390**, 19–26 (2005).
5. T. P. Moskvina and O. D. Sidorova, "Heat treatment of powder metallurgy constructional steel (review)," Metal Sci. Heat Treat. **29**, 270–282 (1987).
6. F. Kafkas, Ç. Karataş, A. Sözen, E. Arcaklioğlu, and S. Sarıtaş, "Determination of residual stresses based on heat treatment conditions and densities on a hybrid (FLN2-4405) powder metallurgy steel using artificial neural network," Mater. Design **28**, 2431–2442 (2007).
7. H. D'Armas, L. Llanes, J. Peñafiel, J. Bas, and M. Anglada, "Tempering effects on the tensile response and fatigue life behavior of a sinter-hardened steel," Mater. Sci. Eng., A **277**, 291–296 (2000).
8. N. Sarıçiçek, "Investigation of mechanical and microstructural properties of austempered powder metal steel," *M. Sc. Thesis,* Gazi Univ., Inst. Sci. Technol. 2012, Ankara, Turkey (in Turkish).
9. M. Campos, J. Sicre-Artalejo, J. J. Muñoz, and J. M. Torralba, "Effect of austempering conditions on the microstructure and tensile properties of low alloyed sintered steel," Metallur. Mater. Trans. A **41**, 1847–1854 (2010).
10. K. Mahesh, S. Sankaran, and P. Venugopal, "Microstructural characterization and mechanical properties of powder metallurgy dual phase steel preforms," J. Mater. Sci. Technol. **28**, 1085–1094 (2012).
11. A. Güral, S. Tekeli, and T. Ando, "Tensile properties of iron-based P/M steels with ferrite plus martensite microstructure," J. Mater. Sci. **41**, 7894–79016 (2006).
12. A. Güral, and M. Türkan, "Comparison of heat treatments on the toughness of 1.7Ni–1.5Cu–0.5Mo prealloyed P/M steels," High Temp. Mater. Process **34**, 271–274 (2015).
13. S. Tekeli, and A. Gural, "Microstructural characterization and impact toughness of intercritically annealed PM steels," Mater. Sci. Eng.ineering A **406**, 172–179 (2005).
14. A. Güral, "Influence of martensite particle size on dry sliding wear behaviour of low carbon dual phase powder metallurgy steels," Kovove Materialy–Metallic Materilas, **48**, 25–31 (2010).
15. L. F. Ramos, D. K. Matlock, and G. Krauss, "Deformation behavior of dual-phase steel," Metallurg. Trans. A – Phys. Metall. Mater. Sci. **10**, 259–261 (1979).
16. G. R. Speich, V. A. Demarest, and R. L. Miller, "Formation of austenite during intercritical annealing of dual-phase steels," Metallurg. Trans. A – Phys. Metall. Mater. Sci. **12**, 1419–1428 (1981).
17. J. Deng, J. Ma, Y. Xu, and Y. Shen, "Effect of martensite distribution on microscopic deformation behavior and mechanical properties of dual phase steels," Acta Metall. Sinica **51**, 1092–1100 (2015).
18. J. Han, S.-J. Lee, C.-Y. Lee, S. Lee, S. Y. Jo, and Y.-K. Lee, "The size effect of initial martensite constituents on the microstructure and tensile properties of intercritically annealed Fe–9Mn–0.05C steel," Mater. Sci. Eng. A **633**, 9–16 (2015).
19. J. Zhang, H. Di, Y. Deng, and R. D. K. Misra, "Effect of martensite morphology and volume fraction on strain hardening and fracture behavior of martensite-ferrite dual phase steel," Mater. Sci. Eng., A **627**, 230–240 (2015).
20. T. Matsuno, D. Maeda, H. Shutoh, A. Uenishi, and M. Suehiro, "Effect of martensite volume fraction on void formation leading to ductile fracture in dual phase steels", ISIJ Int. **54**, 938–944 (2014).
21. S. Gündüz, "Effect of chemical composition, martensite volume fraction and tempering on tensile behaviour of dual phase steels," Mater. Design **63**, 2381–2383 (2009).
22. *ASTM Standard E-8M. Test Methods for Tension Testing of Metallic Materials* Annual Book of ASTM Standards, PA: USA, 1994.
23. N. Chawla, T. F. Murphy, K. S. Narasimhan, M. Koopman, and K. K. Chawla, "Axial fatigue behavior of binder-treated versus diffusion alloyed powder metallurgy steels," Mater. Sci. Eng., A **308**, 180–188 (2001).
24. K. W. Andrew, "Empirical formulae for the calculation of some transformation temperatures," J. Iron and Steel Institute **203**, 721–727 (1965).